Geophysical Research Letters

RESEARCH LETTER
10.1029/2020GL090115

Special Section:
Parker Solar Probe Observations at Venus: VGA1-2

Plasma Double Layers at the Boundary Between Venus and the Solar Wind

D. M. Malaspina[1,2], K. Goodrich[3], R. Livi[3], J. Halekas[4], M. McManus[3], S. Curry[3], S. D. Bale[3,5], J. W. Bonnell[3], T. Dudok de Wit[6], K. Goetz[7], P. R. Harvey[3], R. J. MacDowall[8], M. Pulupa[3], A. W. Case[9], J. C. Kasper[10], K. E. Korreck[9], D. Larson[3], M. L. Stevens[9], and P. Whittlesey[3]

[1]Department of Astrophysical and Planetary Sciences, University of Colorado Boulder, Boulder, CO, USA, [2]Laboratory for Atmospheric and Space Physics, University of Colorado Boulder, Boulder, CO, USA, [3]Space Sciences Laboratory, University of California, Berkeley, CA, USA, [4]Department of Physics and Astronomy, University of Iowa, Iowa City, IA, USA, [5]Physics Department, University of California, Berkeley, CA, USA, [6]LPC2E, CNRS, and University of Orléans, Orléans, France, [7]School of Physics and Astronomy, University of Minnesota, Twin Cities, Minneapolis, MN, USA, [8]NASA Goddard Space Flight Center, Greenbelt, MD, USA, [9]Harvard-Smithsonian Center for Astrophysics, Cambridge, MA, USA, [10]Climate and Space Sciences and Engineering, University of Michigan, Ann Arbor, MI, USA

Key Points:
- Plasma double layers are detected near the Venusian bow shock
- Multiple double layers are identified in a small amount of burst data
- Kinetic processes may help mediate interaction between the solar wind and induced magnetospheres

Correspondence to:
D. M. Malaspina,
David.Malaspina@lasp.colorado.edu

Citation:
Malaspina, D. M., Goodrich, K., Livi, R., Halekas, J., McManus, M., Curry, S., et al. (2020). Plasma double layers at the boundary between Venus and the solar wind. *Geophysical Research Letters*, *47*, e2020GL090115. https://doi.org/10.1029/2020GL090115

Received 30 JUL 2020
Accepted 3 OCT 2020
Accepted article online 9 OCT 2020

Abstract The solar wind is slowed, deflected, and heated as it encounters Venus's induced magnetosphere. The importance of kinetic plasma processes to these interactions has not been examined in detail, due to a lack of constraining observations. In this study, kinetic-scale electric field structures are identified in the Venusian magnetosheath, including plasma double layers. The double layers may be driven by currents or mixing of inhomogeneous plasmas near the edge of the magnetosheath. Estimated double-layer spatial scales are consistent with those reported at Earth. Estimated potential drops are similar to electron temperature gradients across the bow shock. Many double layers are found in few high cadence data captures, suggesting that their amplitudes are high relative to other magnetosheath plasma waves. These are the first direct observations of plasma double layers beyond near-Earth space, supporting the idea that kinetic plasma processes are active in many space plasma environments.

Plain Language Summary Venus has no internally generated magnetic field, yet electric currents running through its ionized upper atmosphere create magnetic fields that push back against the flow of the solar wind. These induced fields cause the solar wind to slow and heat as the flow is deflected around Venus. This work reports observations of very small plasma structures that accelerate particles, identifiable by their characteristic electric field signatures, at the boundary where the solar wind starts to be deflected. These small plasma structures observed at Venus have been studied in near-Earth space for decades but have never before been found near another planet. These structures are known to be important to the physics of strong electrical currents in space plasmas and the blending of dissimilar plasmas. Their identification at Venus is a strong demonstration that these small plasma structures are a universal plasma phenomena, at work in many plasma environments.

1. Introduction

Venus does not have an intrinsic magnetic field. It does have a thick neutral atmosphere that is ionized by solar photons, forming a conducting ionosphere that supports currents. The time-variable interplanetary magnetic field (IMF) drives currents in the ionosphere, which induce magnetic fields to oppose those in the IMF. These induced fields produce a magnetic obstacle to the solar wind, against which the IMF magnetic field "piles-up" and drapes (Futaana et al., 2017, and references therein).

Venus's induced magnetosphere exhibits structures analogous to those found where the solar wind encounters magnetized planets, including a bow shock, magnetosheath, and magnetotail. These structures have significantly different character at Venus than at Earth. At Venus, the upstream bow shock standoff distance is less than one planetary radius from the surface (e.g., Martinecz et al., 2009). At Earth, it is ~12 Earth radii. Knudsen et al. (2016) found that, at Venus, transformation of a significant portion of incident solar wind kinetic energy into ion and electron thermal energy was localized to a thin (100–200 km) layer,

colocated with observations of non-Maxwellian electron distributions and the bow shock magnetic ramp. Pressure from heated sheath electrons, combined with the convective electric field, are important for defining the altitude of the ion composition boundary which separates the solar wind from the planetary plasma (Martinecz et al., 2008).

Both ion and electron foreshocks, due to solar wind particles reflecting at the Venus bow shock, have been identified, and limited exploration of the waves associated with those structures was made using a four-frequency spectrum analyzer on Pioneer Venus Orbiter (Russell et al., 2006) (active 1978–1992). However, identification of specific wave modes was difficult, and few spacecraft with electric field instruments have visited Venus since, all with brief encounters (Futaana et al., 2017). Therefore, the role of kinetic wave-particle interactions in mediating the interaction between the solar wind and Venus's induced magnetosphere has not been comprehensively addressed by observations.

Parker Solar Probe (PSP) uses seven gravitational encounters with Venus to lower its solar orbital periapsis (Fox et al., 2016). The encounters require PSP to pass close to Venus (<1 Venus radii altitude), resulting in passage through its induced magnetosphere. At the time of writing, PSP has returned data from three Venus encounters. This work focuses on the second encounter, which occurred on 26 December 2019.

Several PSP instruments were powered on during the Venus encounters, including FIELDS (Bale et al., 2016). The PSP Venus encounters are the first time that an electric field instrument has visited near-Venus space (Futaana et al., 2017) since two brief encounters with Venus by the Cassini spacecraft in 1998 and 1999 (Gurnett et al., 2001) and the first DC-coupled electric field instrument near Venus since Vega in 1985 (Klimov et al., 1986).

The FIELDS burst data enable relatively long captures of high cadence time series fields data. In near-Earth space, such data enabled observations of kinetic-scale electric field structures, such as electron phase space holes and plasma double layers (e.g., Cattell et al., 2002; Ergun et al., 2001, 2009; Franz et al., 1998; Fu et al., 2020; Holmes et al., 2018; Li et al., 2015; Malaspina et al., 2014; Matsumoto et al., 1994; Mozer et al., 2013; Pickett et al., 2003). These structures characteristically feature strong electric fields parallel to the background magnetic field, and they appear in kinetically unstable plasmas (e.g., Hutchinson, 2017; Schamel, 2012, and references therein), often in association with magnetic field-aligned currents (Ergun et al., 2001; Mozer et al., 2014) or near the interface between two disparate plasma populations as they homogenize (Holmes et al., 2018; Malaspina et al., 2014; Pickett et al., 2004). In near-Earth space, kinetic-scale electric field structures have been identified in virtually every region where significant wave-particle energy transfer occurs and instrumentation capable of observing them is present, including the auroral region (Ergun et al., 2001), plasma sheet (Ergun et al., 2009; Matsumoto et al., 1994), radiation belts (Malaspina et al., 2014; Mozer et al., 2013), magnetosheath (Cattell et al., 2002; Pickett et al., 2003), and bow shock (Goodrich et al., 2018; Li et al., 2015).

While kinetic-scale electric field structures have been identified and studied extensively at Earth, they have not been reported at induced magnetospheres such as Venus or Mars. Double layers in particular have not been reported in any planetary magnetosphere except Earth's. Considering the ubiquity of kinetic-scale electric field structures in the Earth's magnetosphere, and their prominent role in the kinetic physics of magnetic field-aligned currents and plasma homogenization, these structures are very likely to be present in induced planetary magnetospheres but have remained undetected due to the small number of observations capable of detecting them.

In this work, observations of electron phase space holes and plasma double layers at the interface between Venus and the solar wind are reported, and their significance for the near-Venus plasma environment is discussed.

2. Data and Processing

This study makes use of data from the FIELDS (Bale et al., 2016) and SWEAP (Kasper et al., 2016) instrument suites on the PSP spacecraft.

FIELDS measures electric and magnetic fields across a broad frequency range: DC—20 MHz for electric fields and DC—1 MHz for magnetic fields. The electric field sensors consist of four ~2 m antennas in the plane of the heat shield (V_1, V_2, V_3, and V_4) and one ~21 cm antenna mounted on the magnetometer boom

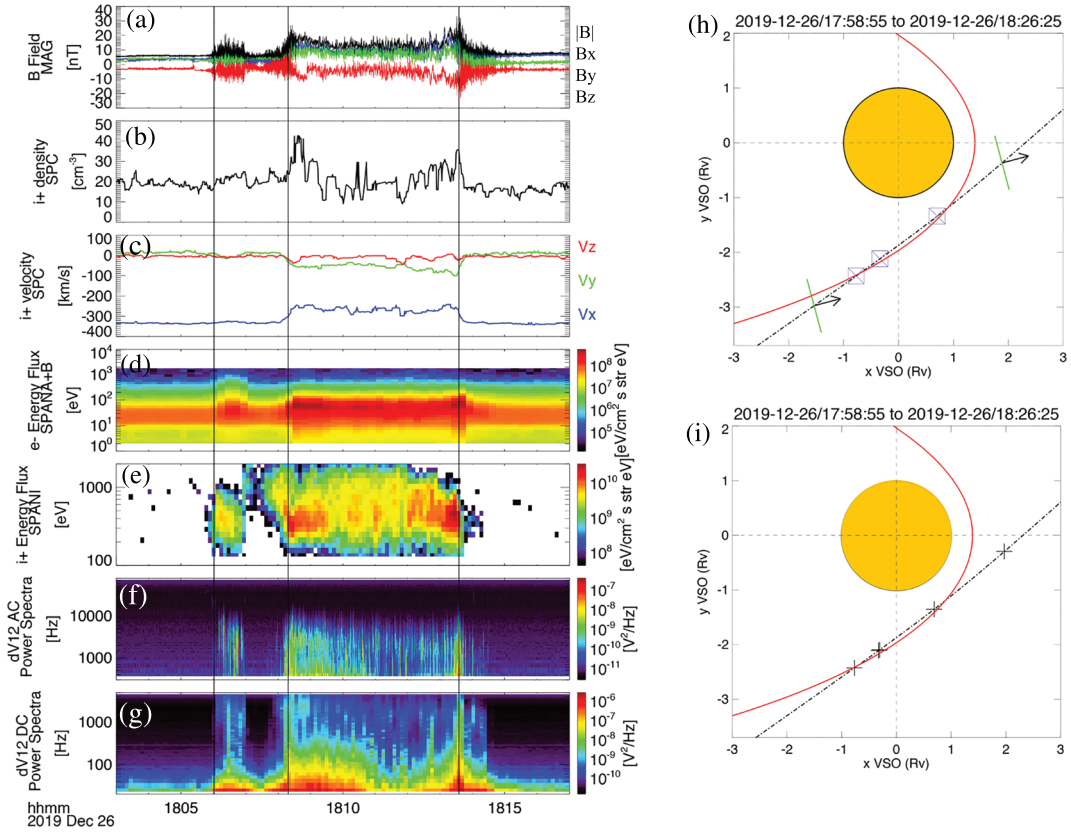

Figure 1. (a) $|B|$ and $\vec{B}$, in VSO coordinates, (b) proton density from SPC, (c) proton flow velocity in VSO from SPC, (d) electron energy flux from SPANe, (e) proton energy flux from SPANi, (f) power spectra of $V_1 - V_2$ differential voltages for ~400 Hz to 75 kHz, (g) same as (f), but for ~20 Hz to ~9.4 kHz, and (h) PSP trajectory (black dashed line) with notional bow shock (red line) and bow shock crossing times (blue boxes). A black arrow shows the outward normal to the heat shield. The green bar shows the heat shield plane. (i) Same as (h), with black crosses indicating burst data capture times.

"tail" of the spacecraft (V_5). The magnetic field sensors include two fluxgate magnetometers (FGM) and one search coil magnetometer (SCM) mounted to the magnetometer boom.

The low-energy particle instrument suite, SWEAP, consists of four detectors: the Solar Probe Cup (SPC), a Faraday cup pointing normal to the heat shield plane (Case et al., 2020), two SPANe electron detectors (Whittlesey et al., 2020), one on either side of the spacecraft but behind the heat shield, and one SPANi ion detector, also behind the heat shield. The SPAN detectors are top hat electrostatic analyzers measuring the distributions of electrons or protons from a few eV to ~30 keV, at a cadence of ~13.98 s for the second Venus encounter. SPC measures protons and alpha particle distributions (~100 eV to ~8 keV), primarily in the direction normal to the heat shield with a cadence of ~0.87 s. SPANi data are used as well when the flow deviates significantly from the SPC field of view (~13.98 s cadence).

The Digital Fields Board (DFB) is a receiver within the FIELDS instrument (Malaspina et al., 2016). DFB burst mode data are important to this study. These data consist of six channels of data recorded at 150,000 samples per second (sps) for intervals of ~3.5 s. During the second Venus encounter, these channels included differential voltages in the heat shield plane ($dV_{12} = V_1 - V_2$ and $dV_{34} = V_3 - V_4$) and three orthogonal axes of SCM data. The differential voltage data are band-pass filtered, with −3 dB points near ~100 Hz and ~60 kHz. The SCM data band-pass response has −3 dB points near ~20 Hz and ~60 kHz.

DFB high cadence data (150,000 sps) are continuously recorded then parsed into ~3.5 s burst data intervals. Each burst data interval is assigned a quality flag, with a value based on peak signal to noise ratio within a given burst interval. These intervals enter a competitive queue. Intervals with the highest quality flags are kept, and others discarded. The competitive queue stores six events at a time and events exit the queue into

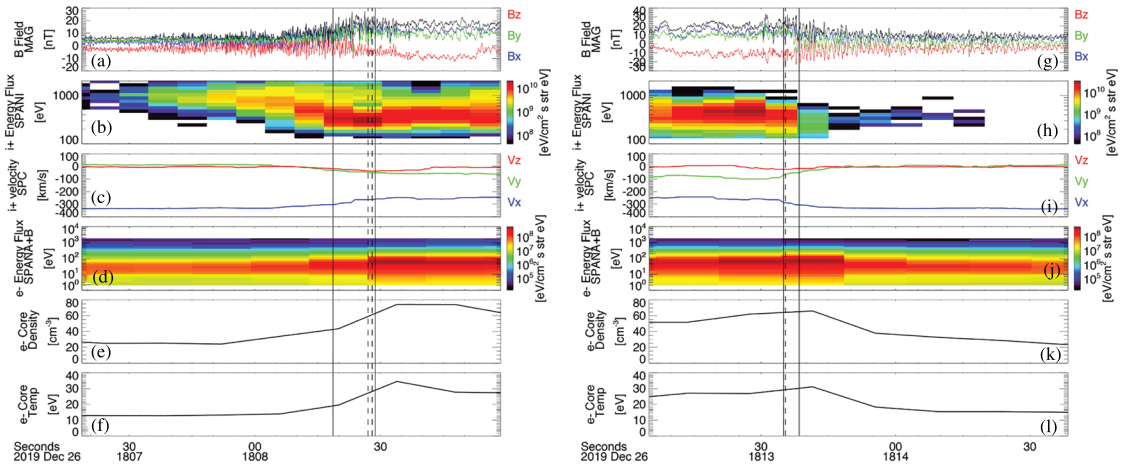

Figure 2. (a) Three components of $\vec{B}$, in VSO coordinates, (b) ion energy flux from SPANi, (c) proton flow velocity in VSO from SPC, (d) electron energy flux from SPANe, and (e and f) electron core density and temperature from fits to SPANe data. (g–l) Same quantities, for outbound bow shock crossing. Vertical solid lines indicate start and stop times of FIELDS burst data, and vertical lines indicate plasma double-layer observations.

the FIELDS onboard memory at the rate of one every ~20 min. This time is on the same order as the duration of the PSP Venus encounter. If a given event has high signal-to-noise compared to subsequently recorded data, that event will persist in the queue until it exits. Based on these considerations, FIELDS is expected to record ~6 DFB burst data intervals within a few Venus radii of the planet, per Venus encounter.

3. Observations

Figure 1 presents an overview of the second PSP Venus encounter. Likely bow shock crossings are indicated by vertical solid lines. A partial bow shock crossing near 18:06 UTC suggests that PSP is skimming the bow shock.

Figure 1a shows the background magnetic field ($\vec{B}$), including relatively steady and weak fields in the solar wind at the start and end of the period, as well as enhanced magnitude and fluctuations where the field piles up against Venus's induced magnetic field. Figure 1b shows proton density (11-point median smoothed), with increases at the solar wind/induced magnetosphere interface. Figure 1c shows proton bulk flow velocity from SPC (11-point median smoothed), with clear slowing and deflection of solar wind plasma. Figure 1d shows electron energy flux, with heating regions visible planetward of each bow shock crossing. Figure 1e shows proton energy flux, with heating features at each bow shock crossing. Figures 1f and 1g show onboard calculated power spectra of differential voltage measurements in the heat shield plane for two frequency ranges. Wave power is strongest and spans the most bandwidth at the bow shock crossings. The magnetic field and particle data from these bow shock crossings are similar to those reported previously (e.g., Fränz et al., 2017; Knudsen et al., 2016; Martinecz et al., 2009)

Figures 1h and 1i show the geometry of the encounter in the x-y Venus Solar Orbital coordinates (VSO) plane. The red curve shows a notional bow shock, modeled as a conic where $r = L/(1 + \epsilon cos(\theta))$. Values for the semilatus rectum L, the eccentricity ϵ, and the conic focus x_0 were chosen by starting with typical values determined by Martinecz et al. (2009) and adjusting them to minimize the distance between the shock surface and the first and last bow shock crossings. The chosen values are $L = 1.45 R_v$, $\epsilon = 0.95$, and $x_0 = 0.64 R_v$. The dash dotted lines show the PSP trajectory from 17:58 to 18:26 UTC. In Figure 1h, black arrows indicate the outward vector normal to the PSP heat shield. The heat shield plane is indicated by green bars. Blue boxes indicate bow shock crossing times (vertical lines in Figures 1a–1d). In Figure 1i black crosses indicate DFB burst data times. Burst captures are triggered by high-amplitude wave activity and cluster near bowshock crossings.

Figure 2 shows plasma condition detail at inbound and outbound crossings of the Venusian bow shock. Figures 2a and 2g show $\vec{B}$ in VSO coordinates, with $|B|$ plotted in black, Figures 2b and 2h show proton energy flux from SPANi, Figures 2c and 2i show proton bulk flow velocity in VSO from SPC (11-point median smoothed), Figures 2d and 2j show electron energy flux from SPANe, and Figures 2e and 2k show electron core density determined by fits to the core of the electron distribution as measured by SPANe

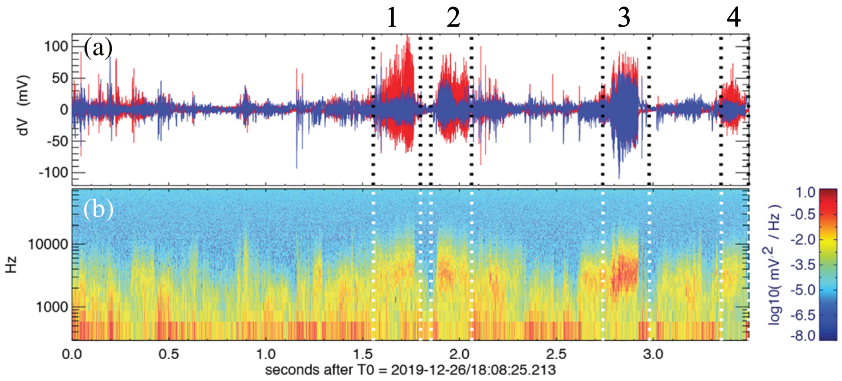

Figure 3. (a) Time series differential voltage waveforms in the heat shield plane, in spacecraft body coordinates. The blue trace indicates spacecraft *x* (close to the ecliptic plane), the red trace spacecraft *y* (close to normal to the ecliptic). Vertical lines indicate intervals with plasma double layers. (b) Windowed Fourier transform of the data in (a).

(following the method of Halekas et al., 2020). Figures 2f and 2l show electron core temperature determined by the same fits.

Vertical solid lines bracket burst data intervals, while vertical dashed lines indicate times when plasma double layers were observed (e.g., Figure 4). Burst data were recorded just planetward of each bow shock ramp, where $|B|$ is enhanced by pile-up, the solar wind is slowed and deflected, and electrons are heated. Protons observed between ~18:07 and ~18:08 UTC and after ~18:13 UTC are likely reflected by interaction with the bow shock. Kinetic-scale electric field structures, including double layers, are embedded in the region where the strongest energy transfer from solar wind ram energy to particle heating and flow deflection occurs.

Figure 3 shows one burst interval dense with plasma double layers. Figure 3a shows differential voltage data from the two antenna pairs in the PSP heat shield plane, rotated into spacecraft body *x*-*y* coordinates. Figure 3b shows a windowed Fourier power spectrum of the data in Figure 3a. Regions of intense high-frequency electrostatic activity are indicated by vertical dashed lines and numbered. When these regions are examined in detail (see Figure 4), plasma double layers with developed two-stream electron instabilities are observed.

Several other electrostatic structures, including phase space holes and double layers without developed instabilities, are also observed during this interval (see Figure 4). Data from the SCM are not shown because they contain only noise for this ~3.5 s interval. The activity in Figure 3 is electrostatic to the sensitivity of the SCM as operated during this encounter.

Figures 4a–4p show waveforms for four double layers with developed streaming instabilities, numbered corresponding to Figure 3. Each double layer is described by four panels, each showing two orthogonal differential voltage signals in the heat shield plane, rotated into a maximum variance coordinate system. The maximum variance direction is determined using the narrow interval around each double layer (gray shading). Each panel shows the maximum variance (top) and perpendicular components (bottom). Figures 4a, 4e, 4i, and 4m show an extended monopolar electric field bounding a region of rapidly oscillating electric field. Figures 4b, 4f, 4j, and 4n, 4c, 4g, 4k, and 4o, and 4d, 4h, 4l, and 4p show electric fields from regions at times indicated by the vertical red lines. In each case, three red vertical lines correspond to the three sets of small plots showing early, middle, and late times in each double-layer example. For example, Figure 4f corresponds to the time indicated by the leftmost red line in Figure 4e. In each case, electric field fluctuations are least structured close to the double layer and progressively evolve into coherent bipolar structures (most evident in Figure 4b and 4h). Figures 4q and 4r are described below.

These observations are consistent with simulated (e.g., Goldman et al., 2008; Newman et al., 2001) and observed (e.g., Andersson et al., 2002; Ergun et al., 2009; Malaspina et al., 2014) doubler-layer-driven two-stream instability, where coherent phase space vortices, recognizable as bipolar electric field pulses (e.g., Figure 4b), form some distance from the double layer.

Additionally, this interval contains ~10 monopolar electric field pulses without developed streaming instability signatures (e.g., Figure 4i, far right). These pulses have their largest amplitude in the maximum

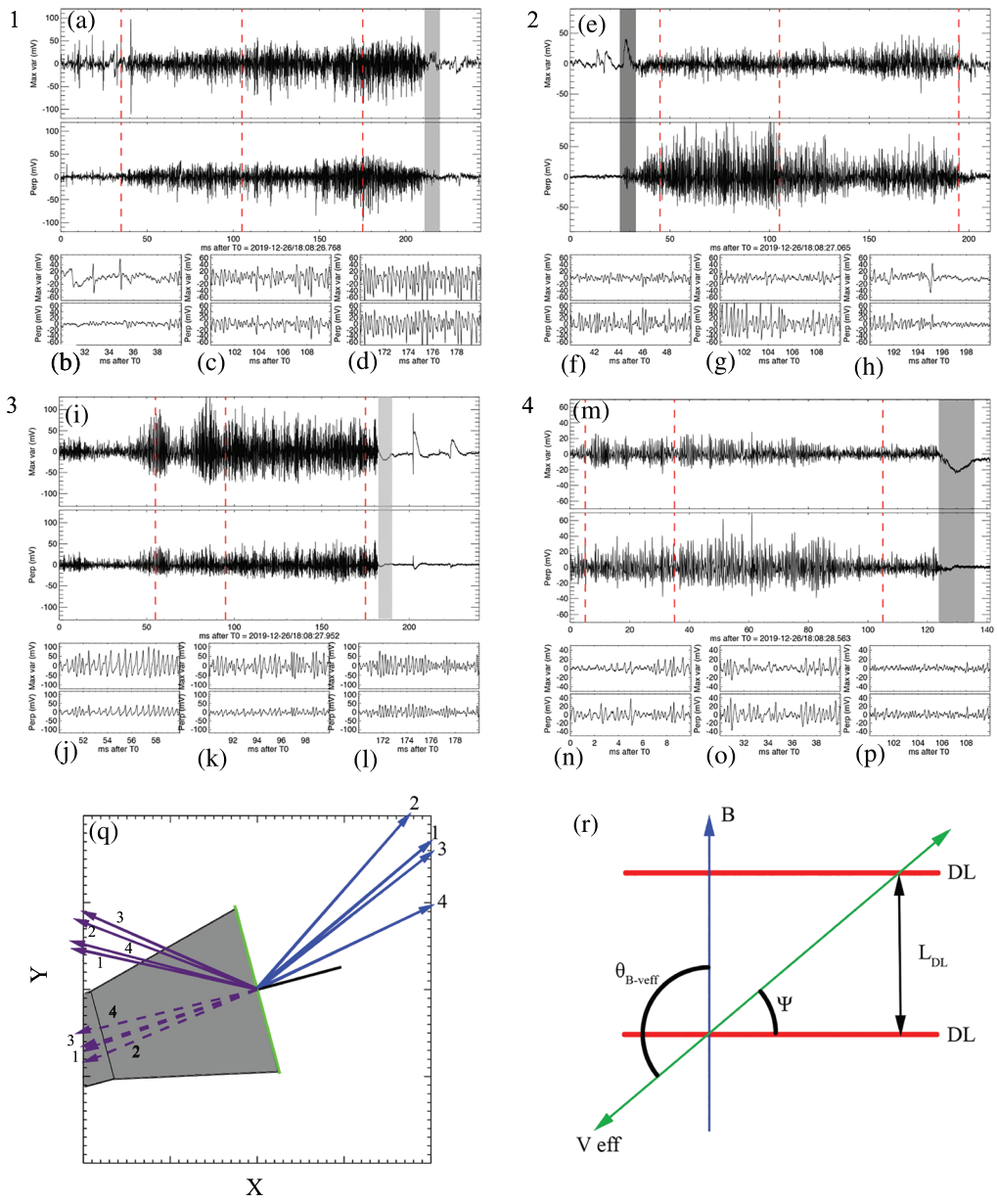

Figure 4. Each pair of panels shows time domain differential voltage data along two directions in the plane of the heat shield: maximum variance (top) and perpendicular (bottom). (a) shows a double layer (gray shading) with attendant electrostatic waves. (b)–(d) show data from subintervals of (a) at times indicated by vertical red lines. (e–h), (i–l), and (m–p) have the same format as (a)–(d) but for thee other double layers. (q) Vectors, for each of the four double layers, projected into the *x*-*y* VSO plane, for the magnetic field (blue), effective double-layer velocity assuming $\vec{v}_{eff} || \vec{B}$ (solid purple) and assuming $\vec{v}_{eff} || -\vec{B}$ (dashed purple). The heat shield plane is shown in green, and its normal vector in black. A cartoon spacecraft bus is shown in gray. (r) Geometry of an oblique double-layer crossing, in a plane containing $\vec{B}$ (blue) and $\vec{v}_{eff}$ (green).

variance coordinate system defined by the identified double layers, consistent with the interpretation that they are also double layers.

The spatial scale and potential drop associated with each double layer in Figure 4 can be estimated. To do so, it is assumed (following Ergun et al., 2009) that the double layers propagate parallel or antiparallel to the background magnetic field direction ($\hat{B}$) at the ion sound speed (c_s). The effective velocity of the double layer in the frame of the spacecraft (v_{eff}) is therefore $\vec{v}_{eff} = (\pm c_s \hat{B}) + \vec{v}_{sc} + \vec{v}_p$, where $\vec{v}_{sc}$ is the spacecraft velocity and $\vec{v}_p$ is the proton bulk flow velocity. Here, all velocities are in VSO coordinates. Because each of these

velocities (c_s, v_{sc}, v_p) is of similar magnitude, it is likely that the spacecraft encounters the double layer at an oblique angle. Figure 4r shows this geometry in the plane defined by $\hat{B}$ and $\vec{v}_{eff}$. The double-layer width is then $L_{DL} = |v_{eff}|\, dt_{DL}\, sin(\psi)$. ψ is defined as $\theta_{B,veff} - 90°$, where $\theta_{B,veff}$ is the angle between the background magnetic field direction and the effective velocity vector. Because it is not known a priori whether the double layer is propagating along $\hat{B}$ or $-\hat{B}$, two L_{DL} results are possible for each double layer.

For Double Layers 1–4 in Figure 4, estimated L_{DL} are $37\lambda_D$, $62\lambda_D$, $71\lambda_D$, and $155\lambda_D$, respectively, for Debye length λ_D. Here, $\vec{v}_p$ and the proton temperature are defined using the SPC sample closest in time to each double layer. SPANi proton core distribution fitting indicates a maximum flow deviation of ~13° from the spacecraft z axis, and SPC data are valid for flows ±30° from spacecraft z (Kasper et al., 2016); therefore, we use SPC data for ion properties. Electron core density and temperature are derived from fits to SPANe data (following Halekas et al., 2020).

The estimated spatial scales (few tens of Debye lengths) are consistent with prior studies at Earth (e.g., Ergun et al., 2009, and references therein), except for the fourth double layer, which is a factor of 2 or 3 larger than expected. Figure 4q shows $\hat{B}$ (blue) and $\hat{v}_{eff}$ for propagation along $\hat{B}$ (purple solid) and $-\hat{B}$ (purple dashed), with respect to the heat shield plane (green), with all vectors projected into the x-y VSO plane. Reasonable values for L_{DL} require propagation along $\hat{B}$ (generally away from Venus). Assuming propagation along $-\hat{B}$ results in $L_{DL} >> 500\ \lambda_D$, which is too large to maintain charge separation.

Each double layer's potential drop can be estimated as $\Phi = \int E_{||} dl$, where $\int E_{||} dl = (\int E_{||} dt) \cdot (|v_{eff}| sin(\psi))$ where dt is the inverse sample rate. Only the projection of $E_{||}$ in the heat shield plane can be measured accurately, but $E_{||}$ can be estimated as $E_{measured}/cos(\theta_{Bxy})$, where θ_{Bxy} is the angle between $\vec{B}$ and the heat shield plane (x-y plane in spacecraft coordinates). A further complication is that the effective electrical length of the antenna is unknown at these frequencies at this time. Therefore, it is useful to define, $E_{measured} = -dV_{measured}/L_{eff}$ for the differential voltage measurements (dV) shown in Figure 4. Assuming $L_{eff} \approx 1$ m, and integrating over the gray regions marked for the four double layers, the potential drops are estimated to be $\Phi = 13$, 9, 32, and 86 V. A longer effective electrical length linearly reduces the potential drop estimates. Given the approximations used, additional precision on the voltage drop estimates is not meaningful.

These potential drops, except possibly the fourth, are similar to the electron temperature gradient across the bow shock (Figure 2), leaving open the possibility that these double layers are either (i) formed as hot sheath electrons mix with cold solar wind electrons or (ii) accelerating solar wind electrons to a significant fraction of the sheath temperature as they encounter the double-layer electric potential. Future studies are required to evaluate these scenarios. The first possibility is consistent with simulations of double layers separating hot and cold electron populations, which have found that double-layer potential drops can be limited by the hot electron temperature (Li et al., 2013).

4. Discussion

The plasma double layers and associated kinetic-scale electric field structures are observed just planetward of the bow shock magnetic ramp, a narrow spatial region where solar wind particles are undergo deceleration, deflection and heating. A study by Knudsen et al. (2016) explored this region with data from Pioneer Venus, inferring that "… non-Maxwellian … electron velocity distributions colocated with the magnetic field ramp occur in a continuous but convoluted layer of the order of 100 to 200 km thick". The current observations of kinetic plasma structures within the shock ramp are entirely consistent with this, and double layers naturally explain the presence of non-Maxwellian electron velocity distributions.

FIELDS returned five ~3.5 s DFB burst captures during the ~15 min second Venus encounter. Four were recorded as the spacecraft skimmed the bow shock and two contained signatures of plasma double layers. Even with this limited data set, at least six double layers with active streaming instabilities (four shown here), and at least ten likely double layers without streaming instabilities, were observed. By comparison, decades of burst captured by missions traversing Earth's bow shock (Geotail, Cluster, THEMIS, and MMS) yielded two published observations of double layers (Goodrich et al., 2018; Li et al., 2015). Li et al. (2015) identified nine distinct double layers in one shock crossing. Goodrich et al. (2018) identified one double layer in one shock crossing.

One possible explanation relates to how plasma waves at Earth and Venus interact with burst data capture systems. Fields data burst capture systems are generally configured to trigger on the largest-amplitude signals in a given interval. This is true for both near-Earth missions and PSP at Venus. Near Earth's bow shock, there are many high-amplitude, high-frequency waves (e.g., Wilson et al., 2014, and references therein) to trigger burst captures. Structures like double layers are lower amplitude and therefore are less likely to trigger a capture. If, at Venus, double layers and the electrostatic waves they drive have amplitudes higher than other shock- and sheath-driven high-frequency waves (consistent with Figures 1f and 1g), they would be preferentially selected by the burst trigger algorithm.

The estimated spatial scales and potential drops are consistent with prior studies (e.g., Ergun et al., 2009, and references therein) for three of the four double layers investigated. Estimates for the fourth are too large and too deep, possibly due to the steep angle of $\hat{B}$ with respect to the heat shield (Figure 4q), for which measurements in the heat shield plane are less representative of the parallel electric field, or possibly due to underestimate of effective electrical length.

5. Conclusions

This work reports the first observation of a plasma double layer outside of near-Earth space and the first observations of kinetic-scale electric field structures at Venus's induced magnetosphere. The morphology of the time series data, estimated spatial scales, and estimated potential depths is all consistent with observations of double layers observed in Earth's magnetosphere. These structures are observed on the planetward side of the bow shock magnetic ramp, where solar wind particles are being slowed, deflected, and heated. Their presence demonstrates that kinetic plasma physics processes are active in the slowing, deflection, and heating of solar wind particles at the Venus-induced magnetosphere. Observations of these structures on future PSP Venus encounters or by a future Venus space plasma investigation may help determine whether double layers at the Venus bow shock are driven by field-aligned currents within the draped IMF magnetic field lines or by the mixing of solar wind and magnetosheath plasma. Finally, the observations reported here imply that kinetic-scale plasma phenomena, and in particular structures with parallel electric fields, are likely active in plasma environments with significant wave-particle energy transfer, even if they have not yet been observed.

Data Availability Statement

All data used here are available on the FIELDS and SWEAP data archives (http://fields.ssl.berkeley.edu/data/ and http://sweap.cfa.harvard.edu/pub/data/sci/sweap/).

Acknowledgments
The authors thank the Parker Solar Probe, FIELDS, and SWEAP teams. The FIELDS experiment on Parker Solar Probe was designed and developed under NASA contract NNN06AA01C. T. D. acknowledges support from CNES.

References

Andersson, L., Ergun, R. E., Newman, D. L., McFadden, J. P., Carlson, C. W., & Su, Y. J. (2002). Characteristics of parallel electric fields in the downward current region of the aurora. *Physics of Plasmas*, *9*, 3600–3609. https://doi.org/10.1063/1.1490134

Bale, S. D., Goetz, K., Harvey, P. R., Turin, P., Bonnell, J. W., Dudok de Wit, T., et al. (2016). The FIELDS Instrument suite for Solar Probe Plus. Measuring the coronal plasma and magnetic field, plasma waves and turbulence, and radio signatures of solar transients. *Space Science Reviews*, *204*(1–4), 49–82. https://doi.org/10.1007/s11214-016-0244-5

Case, A. W., Kasper, J. C., Stevens, M. L., Korreck, K. E., Paulson, K., Daigneau, P., et al. (2020). The Solar Probe Cup on the Parker Solar Probe. *The Astrophysical Journal Supplement*, *246*(2), 43. https://doi.org/10.3847/1538-4365/ab5a7b

Cattell, C., Crumley, J., Dombeck, J., Wygant, J. R., & Mozer, F. S. (2002). Polar observations of solitary waves at the Earth's magnetopause. *Geophysical Review Letters*, *29*(5), 1065. https://doi.org/10.1029/2001GL014046

Ergun, R. E., Andersson, L., Tao, J., Angelopoulos, V., Bonnell, J., McFadden, J. P., et al. (2009). Observations of double layers in Earth's plasma sheet. *Physical Review Letters*, *102*(15), 155002. https://doi.org/10.1103/PhysRevLett.102.155002

Ergun, R. E., Su, Y. J., Andersson, L., Carlson, C. W., McFadden, J. P., Mozer, F. S., et al. (2001). Direct observation of localized parallel electric fields in a space plasma. *Physical Review Letters*, *87*(4), 045003. https://doi.org/10.1103/PhysRevLett.87.045003

Fox, N. J., Velli, M. C., Bale, S. D., Decker, R., Driesman, A., Howard, R. A., et al. (2016). The Solar Probe Plus mission: Humanity's first visit to our star. *Space Science Reviews*, *204*(1–4), 7–48. https://doi.org/10.1007/s11214-015-0211-6

Fränz, M., Echer, E., Marques de Souza, A., Dubinin, E., & Zhang, T. L. (2017). Ultra low frequency waves at Venus: Observations by the Venus Express spacecraft. *Planetary and Space Sciences*, *146*, 55–65. https://doi.org/10.1016/j.pss.2017.08.011

Franz, J. R., Kintner, P. M., & Pickett, J. S. (1998). POLAR observations of coherent electric field structures. *Geophysical Research Letters*, *25*, 1277–1280. https://doi.org/10.1029/98GL50870

Fu, H. S., Chen, F., Chen, Z. Z., Xu, Y., Wang, Z., Liu, Y. Y., et al. (2020). First measurements of electrons and waves inside an electrostatic solitary wave. *Physical Review Letters*, *124*, 095101. https://doi.org/10.1103/PhysRevLett.124.095101

Futaana, Y., Stenberg Wieser, G., Barabash, S., & Luhmann, J. G. (2017). Solar wind interaction and impact on the Venus atmosphere. *Space Science Reviews*, *212*(3–4), 1453–1509. https://doi.org/10.1007/s11214-017-0362-8

Goldman, M. V., Newman, D. L., & Pritchett, P. (2008). Vlasov simulations of electron holes driven by particle distributions from PIC reconnection simulations with a guide field. *Geophysical Research Letters*, *35*, L22109. https://doi.org/10.1029/2008GL035608

Goodrich, K. A., Ergun, R., Schwartz, S. J., Wilson, L. B., Newman, D., Wilder, F. D., et al. (2018). MMS observations of electrostatic waves in an oblique shock crossing. *Journal of Geophysical Research: Space Physics*, *123*, 9430–9442. https://doi.org/10.1029/2018JA025830

Gurnett, D. A., Zarka, P., Manning, R., Kurth, W. S., Hospodarsky, G. B., Averkamp, T. F., et al. (2001). Non-detection at Venus of high-frequency radio signals characteristic of terrestrial lightning. *Nature*, *409*(6818), 313–315.

Halekas, J. S., Whittlesey, P., Larson, D. E., McGinnis, D., Maksimovic, M., Berthomier, M., et al. (2020). Electrons in the Young Solar Wind: First Results from the Parker Solar Probe. *The Astrophysical Journal Supplement*, *246*(2), 22. https://doi.org/10.3847/1538-4365/ab4cec

Holmes, J. C., Ergun, R. E., Newman, D. L., Ahmadi, N., Andersson, L., Le Contel, O., et al. (2018). Electron phase-space holes in three dimensions: Multispacecraft observations by magnetospheric multiscale. *Journal of Geophysical Research: Space Physics*, *123*, 9963–9978. https://doi.org/10.1029/2018JA025750

Holmes, J. C., Ergun, R. E., Newman, D. L., Wilder, F. D., Sturner, A. P., Goodrich, K. A., et al. (2018). Negative potential solitary structures in the magnetosheath with large parallel width. *Journal of Geophysical Research: Space Physics*, *123*, 132–145. https://doi.org/10.1002/2017JA024890

Hutchinson, I. H. (2017). Electron holes in phase space: What they are and why they matter. *Physics of Plasmas*, *24*(5), 055601. https://doi.org/10.1063/1.4976854

Kasper, J. C., Abiad, R., Austin, G., Balat-Pichelin, M., Bale, S. D., Belcher, J. W., et al. (2016). Solar Wind Wlectrons Alphas and Protons (SWEAP) investigation: Design of the solar wind and coronal plasma instrument suite for Solar Probe Plus. *Space Science Reviews*, *204*(1–4), 131–186. https://doi.org/10.1007/s11214-015-0206-3

Klimov, S., Savin, S., Sokolov, A., Oberc, P., Orlowski, D., & Woźniak, D. (1986). First results of the VEGA low-frequency plasma wave analyser APV-N. In *Field, particle and wave experiments on cometary missions* (pp. 169–174).

Knudsen, W. C., Jones, D. E., Peterson, B. G., & Knadler, C. E. (2016). Measurement of solar wind electron density and temperature in the shocked region of Venus and the density and temperature of photoelectrons within the ionosphere of Venus. *Journal of Geophysical Research: Space Physics*, *121*, 7753–7770. https://doi.org/10.1002/2016JA022526

Li, T. C., Drake, J. F., & Swisdak, M. (2013). Coronal electron confinement by double layers. *The Astrophysical Journal*, *778*(2), 144. https://doi.org/10.1088/0004-637X/778/2/144

Li, S., Zhang, S., Cai, H., Bai, X., & Xie, Q. (2015). Characteristics of the double layer associated with terrestrial bow shock by THEMIS observation. *Science China Earth Sciences*, *58*(4), 562–572. https://doi.org/10.1007/s11430-014-5040-z

Malaspina, D. M., Andersson, L., Ergun, R. E., Wygant, J. R., Bonnell, J. W., Kletzing, C., et al. (2014). Nonlinear electric field structures in the inner magnetosphere. *Geophysical Review Letters*, *41*, 5693–5701. https://doi.org/10.1002/2014GL061109

Malaspina, D. M., Ergun, R. E., Bolton, M., Kien, M., Summers, D., Stevens, K., et al. (2016). The Digital Fields Board for the FIELDS instrument suite on the solar probe plus mission: Analog and digital signal processing. *Journal of Geophysical Research: Space Physics*, *121*, 5088–5096. https://doi.org/10.1002/2016JA022344

Martinecz, C., Boesswetter, A., FräNz, M., Roussos, E., Woch, J., Krupp, N., et al. (2009). Plasma environment of Venus: Comparison of Venus Express ASPERA-4 measurements with 3-D hybrid simulations. *Journal of Geophysical Research*, *114*, E00B30. https://doi.org/10.1029/2008JE003174

Martinecz, C., Fränz, M., Woch, J., Krupp, N., Roussos, E., Dubinin, E., et al. (2008). Location of the bow shock and ion composition boundaries at Venus—Initial determinations from Venus Express ASPERA-4. *Planetary and Space Sciences*, *56*(6), 780–784. https://doi.org/10.1016/j.pss.2007.07.007

Matsumoto, H., Kojima, H., Miyatake, T., Omura, Y., Okada, M., Nagano, I., & Tsutsui, M. (1994). Electrotastic Solitary Waves (ESW) in the magnetotail: BEN wave forms observed by GEOTAIL. *Geophysical Research Letters*, *21*, 2915–2918. https://doi.org/10.1029/94GL01284

Mozer, F. S., Agapitov, O., Krasnoselskikh, V., Lejosne, S., Reeves, G. D., & Roth, I. (2014). Direct observation of radiation-belt electron acceleration from electron-volt energies to megavolts by nonlinear whistlers. *Physical Review Letters*, *113*(3), 035001. https://doi.org/10.1103/PhysRevLett.113.035001

Mozer, F. S., Bale, S. D., Bonnell, J. W., Chaston, C. C., Roth, I., & Wygant, J. (2013). Megavolt parallel potentials arising from double-layer streams in the Earth's outer radiation belt. *Physical Review Letters*, *111*(23), 235002. https://doi.org/10.1103/PhysRevLett.111.235002

Newman, D. L., Goldman, M. V., Ergun, R. E., & Mangeney, A. (2001). Formation of double layers and electron holes in a current-driven space plasma. *Physical Review Letters*, *87*(25), 255001. https://doi.org/10.1103/PhysRevLett.87.255001

Pickett, J., Chen, L., Kahler, S., Santolík, O., Gurnett, D., Tsurutani, B., & Balogh, A. (2004). Isolated electrostatic structures observed throughout the Cluster orbit: relationship to magnetic field strength. *Annales Geophysicae*, *22*, 2515–2523. https://doi.org/10.5194/angeo-22-2515-2004

Pickett, J. S., Menietti, J. D., Gurnett, D. A., Tsurutani, B., Kintner, P. M., Klatt, E., & Balogh, A. (2003). Solitary potential structures observed in the magnetosheath by the Cluster spacecraft. *Nonlinear Processes in Geophysics*, *10*, 3–11.

Russell, C. T., Luhmann, J. G., & Strangeway, R. J. (2006). The solar wind interaction with Venus through the eyes of the Pioneer Venus Orbiter. *Planetary and Space Sciences*, *54*(13–14), 1482–1495. https://doi.org/10.1016/j.pss.2006.04.025

Schamel, H. (2012). Cnoidal electron hole propagation: Trapping, the forgotten nonlinearity in plasma and fluid dynamics. *Physics of Plasmas*, *19*(2), 020501. https://doi.org/10.1063/1.3682047

Whittlesey, P. L., Larson, D. E., Kasper, J. C., Halekas, J., Abatcha, M., Abiad, R., et al. (2020). Electrons on the Parker Solar Probe. *The Astrophysical Journal Supplement*, *246*(2), 74. https://doi.org/10.3847/1538-4365/ab7370

Wilson, L. B., Sibeck, D. G., Breneman, A. W., Le Contel, O., Cully, C., Turner, D. L., et al. (2014). Quantified energy dissipation rates in the terrestrial bow shock: 2. Waves and dissipation. *Journal of Geophysical Research: Space Physics*, *119*, 6475–6495. https://doi.org/10.1002/2014JA019930